The dual developmental origin of spinal cerebrospinal fluid-contacting neurons gives rise to distinct functional subtypes

Lydia Djenoune, Laura Desban, Johanna Gomez, Jenna R. Sternberg, Andrew Prendergast, Dominique Langui, Feng B. Quan, Hugo Marnas, Thomas O. Auer, Jean-Paul Rio, et al.

▶ **To cite this version:**

Lydia Djenoune, Laura Desban, Johanna Gomez, Jenna R. Sternberg, Andrew Prendergast, et al.. The dual developmental origin of spinal cerebrospinal fluid-contacting neurons gives rise to distinct functional subtypes. Scientific Reports, 2017, 7 (1), pp.719. 10.1038/s41598-017-00350-1 . hal-01516797

HAL Id: hal-01516797

https://hal.sorbonne-universite.fr/hal-01516797v1

Submitted on 2 May 2017

HAL is a multi-disciplinary open access archive for the deposit and dissemination of scientific research documents, whether they are published or not. The documents may come from teaching and research institutions in France or abroad, or from public or private research centers.

L'archive ouverte pluridisciplinaire **HAL**, est destinée au dépôt et à la diffusion de documents scientifiques de niveau recherche, publiés ou non, émanant des établissements d'enseignement et de recherche français ou étrangers, des laboratoires publics ou privés.

Distributed under a Creative Commons Attribution 4.0 International License

SCIENTIFIC REPORTS

OPEN

The dual developmental origin of spinal cerebrospinal fluid-contacting neurons gives rise to distinct functional subtypes

Received: 11 October 2016
Accepted: 30 January 2017
Published online: 07 April 2017

Lydia Djenoune[1,2], Laura Desban[1], Johanna Gomez[1], Jenna R. Sternberg[1], Andrew Prendergast[1], Dominique Langui[1], Feng B. Quan[1,2], Hugo Marnas[1], Thomas O. Auer[3,4], Jean-Paul Rio[1], Filippo Del Bene[3], Pierre-Luc Bardet[1] & Claire Wyart[1]

Chemical and mechanical cues from the cerebrospinal fluid (CSF) can affect the development and function of the central nervous system (CNS). How such cues are detected and relayed to the CNS remains elusive. Cerebrospinal fluid-contacting neurons (CSF-cNs) situated at the interface between the CSF and the CNS are ideally located to convey such information to local networks. In the spinal cord, these GABAergic neurons expressing the PKD2L1 channel extend an apical extension into the CSF and an ascending axon in the spinal cord. In zebrafish and mouse spinal CSF-cNs originate from two distinct progenitor domains characterized by distinct cascades of transcription factors. Here we ask whether these neurons with different developmental origins differentiate into cells types with different functional properties. We show in zebrafish larva that the expression of specific markers, the morphology of the apical extension and axonal projections, as well as the neuronal targets contacted by CSF-cN axons, distinguish the two CSF-cN subtypes. Altogether our study demonstrates that the developmental origins of spinal CSF-cNs give rise to two distinct functional populations of sensory neurons. This work opens novel avenues to understand how these subtypes may carry distinct functions related to development of the spinal cord, locomotion and posture.

The cerebrospinal fluid (CSF) is a complex solution circulating around the central nervous system (CNS). It has classically been assumed that the CSF ensures the homeostasis of the CNS[1]. Multiple studies indicate that the CSF also conveys signals affecting the development and output functions of the CNS, such as feeding, sleep, and locomotion[2–6]. These observations suggest that chemical or mechanical cues from the CSF may act on neurons in the brain and spinal cord. Cerebrospinal fluid-contacting neurons (CSF-cNs) are precisely located at the interface between the CSF and the neuronal circuits[7,8]. In the vertebrate spinal cord, CSF-cNs reside around the central canal[9–15] and project an apical extension in contact with the CSF[8,16–18] and have a locally-projecting axon[14,19,20] that contacts other spinal neurons[12,15,21].

One essential step to understand spinal CSF-cN functions lies in identifying specific markers for these cells. In this regard, the polycystic kidney disease 2 like 1 (PKD2L1) channel also called TRPP3[22], which belongs to the Transient Potential Receptor (TRP) family, appears as a robust candidate to label CSF-cNs[11,13,23,24]. PKD2L1, originally identified as the sour taste receptor in the taste buds, has been found in the spinal CSF-cNs of mouse[11,13,25,26], zebrafish and macaques[13]. The opening of the PKD2L1 channel is modulated by variations in pH[27] and osmolarity[28]. Although the physiological variations of pH and osmolarity in the CSF are not well known, these observations suggest that CSF-cNs could be interoceptors modulated by chemical and/or mechanical cues from the CSF[23].

[1]Sorbonne Universités, UPMC Univ Paris 06, Inserm, CNRS, AP-HP, Institut du Cerveau et de la Moelle épinière (ICM) - Hôpital Pitié-Salpêtrière, Boulevard de l'hôpital, F-75013, Paris, France. [2]Muséum National d'Histoire Naturelle, Paris, 75005, France. [3]Institut Curie, Paris, 75005, France. [4]Present address: Thomas O Auer, Center for Integrative Genomics, Faculty of Biology and Medicine, University of Lausanne, Lausanne, Switzerland. Correspondence and requests for materials should be addressed to P.-L.B. (email: pierreluc.bardet@icm-institute.org) or C.W. (email: claire.wyart@icm-institute.org)

There is evidence that spinal CSF-cNs do not constitute a homogeneous population of neurons. In particular, these cells originate from distinct progenitor domains and are specified differentially by several cascades of transcription factors[26,29–32]. In zebrafish, CSF-cNs are subdivided into the ventral population, referred to as KA", originating from the progenitor domain p3 and a dorsal population, referred to as KA', originating from pMN[29,30]. In mouse, spinal CSF-cNs were recently shown to originate from the p3 and p2 progenitor domains[26]. In addition, some secreted compounds have been previously reported in a restricted number of spinal CSF-cNs, such as the somatostatin[33,34] or serotonin[35,36].

The zebrafish has emerged as an ideal model organism to study the development[13,29,30], the morphology and physiological roles of CSF-cNs *in vivo* due to its transparency at early stages[12,15,37]. Yet, few functional markers of CSF-cNs related to their sensory or secretory functions have been identified in this species. Here, we investigate whether the two types of spinal CSF-cNs defined by distinct developmental origins can be discriminated by morphology, projection on neuronal targets and expression of secreted compounds. Using a quantitative measure of cell shape, we show that ventral and dorsal CSF-cNs have differently shaped apical extensions as well as different axonal projections and consequently project onto distinct neuronal targets within the spinal cord. By electron microscopy (EM), we found that both populations of CSF-cNs exhibit large granular vesicles in accordance with secretory properties. We demonstrate that these two cell types express distinct modulators and peptides: while ventral CSF-cNs transiently express serotonin, dorsal CSF-cNs express the *sst1.1* somatostatin paralog. We observed that the Pkd2l1 channel is not required for the differentiation of CSF-cN axonal projections, for the expression of serotonin or somatostatin. Altogether, our results show that spinal CSF-cNs constitute two distinct functional cell types that differ in apical and axonal morphology, neuronal targets within the spinal cord as well as in the transient expression of secreted compounds.

Results

CSF-cNs are neurosecretory cells with an apical extension into the central canal. We characterized CSF-cN ultrastructure in transverse sections of the 2.5 days post fertilization (dpf) zebrafish spinal cord by transmission electron microscopy (TEM). Without specific markers, we observed cells around the central canal that bore an apical extension with microvilli (Supplemental Fig. 1). To demonstrate these cells were CSF-cNs, we transiently expressed the engineered genetically-encoded peroxidase APEX2 under the *pkd2l1* promoter (see Materials and Methods, Supplemental Fig. 2). In APEX2-TagRFP^{+} larvae, we performed diaminobenzidine (DAB) staining (see Material and Methods, and Supplemental Fig. 3). DAB was detected only within CSF-cNs in the spinal cord, making the cells appear darker (Supplemental Fig. 3b). The specific DAB staining (Figs 1 and 2) revealed that CSF-cNs were either round (Figs 1a and 2a-b) or pear-shaped (Fig. 1b). Ventral and dorsal CSF-cNs bear an apical extension with several microvilli directed toward the lumen of the central canal (Figs 1c and 2c). Among actin-based microvilli, we observed, as previously described in one cell[37], a single cilium directed toward the CSF (Fig. 1d, n = 12 ventral CSF-cNs, Fig. 2d, n = 3 dorsal CSF-cNs). This cilium bears two central microtubule singlets along the axoneme (Figs 1d and 2d-e), often seen in a kinocilium[38,39]. In APEX2^{+} CSF-cNs, we observed large granular vesicles (Figs 1e and 2f), suggesting that these cells either release or uptake peptides or neuromodulators into or from the CSF. Interestingly, we observed one axo-somatic symmetric synaptic contact at the basal pole of a CSF-cN (Fig. 1f), suggesting that CSF-cNs receive inhibitory synaptic inputs. Indeed, asymmetric synapses usually contain glutamate, are non-GABA immunoreactive and are therefore considered excitatory, while symmetric synapses contain GABA and are considered inhibitory[40–42]. Altogether, our TEM data show that both populations of CSF-cNs exhibit properties of sensory and secretory cells.

CSF-cNs display different shapes of apical extensions and axonal projections. As a quantitative analysis of CSF-cN morphology is difficult using serial EM, we turned to fluorescence for a quantitative comparison of the apical extension and the axonal projections of dorsal and ventral CSF-cNs. First, we tested whether these cells differ in the morphology of their apical extension. We investigated the shape of the CSF-cN apical extension by labeling the membrane of CSF-cNs in *Tg*(*pkd2l1*:*Gal4*;*UAS*:*TagRFPCAAX*;*cmlc2*:*eGFP*)*icm22* larvae or F-actin itself in *Tg*(*pkd2l1*:*Gal4*;*UAS*:*LifeAct-GFP*;*cryaa*:*V*)*icm28* larvae or larvae transiently expressing (*pkd2l1*:*Gal4*) and (*UAS*:*LifeAct-TagRFP*;*cryaa*:*C*). Using these different approaches, we found that the shape of the apical extension differs between ventral and dorsal CSF-cNs at 3 and 6 dpf (Fig. 3a,b and Material and Methods). The apical extension of dorsal CSF-cNs (Fig. 3a,b) was more extended along the border of the central canal than for ventral cells (Fig. 3a,b). The apical extension in ventral CSF-cNs was overall more compact with a small proportion displaying a more extended apical extension similar to dorsal CSF-cNs (13.3%, n = 6 out of 45 ventral CSF-cNs, Fig. 3a, empty arrow). Next, to assess whether ventral and dorsal CSF-cNs differ in their axonal projections, we injected the (*pkd2l1-TagRFP*) DNA construct to label single cells (Supplemental Fig. 4a) and reconstructed their axon (Fig. 3c, Supplemental Fig. 4b,c). All CSF-cN axonal projections were ventral, ipsilateral and ascending, yet they were heterogeneous along the rostrocaudal axis of the spinal cord (n = 54, Fig. 3c). We measured significant differences between the axonal projections of the two populations of CSF-cNs in terms of the area of the axonal arborization, the length of the axon, the dorso-ventral coverage within the spinal cord and the number of axonal branches (Fig. 3d). The larger axonal length, arborization and number of branches in ventral CSF-cNs compared to dorsal cells suggest these ventral cells possibly differentiate before dorsal ones. Nonetheless, the fact that the dorsal and ventral populations of CSF-cNs project on different domains along the dorso-ventral axis of the spinal cord suggests that these two populations may target different neuronal types within the ventral spinal cord.

Distinct neuronal targets for ventral and dorsal CSF-cNs within the spinal cord. Differences in the axonal projection of ventral and dorsal CSF-cNs suggest these cells may project onto distinct targets within the spinal cord. Our lab recently demonstrated that CSF-cNs project onto caudal primary (CaP) motor

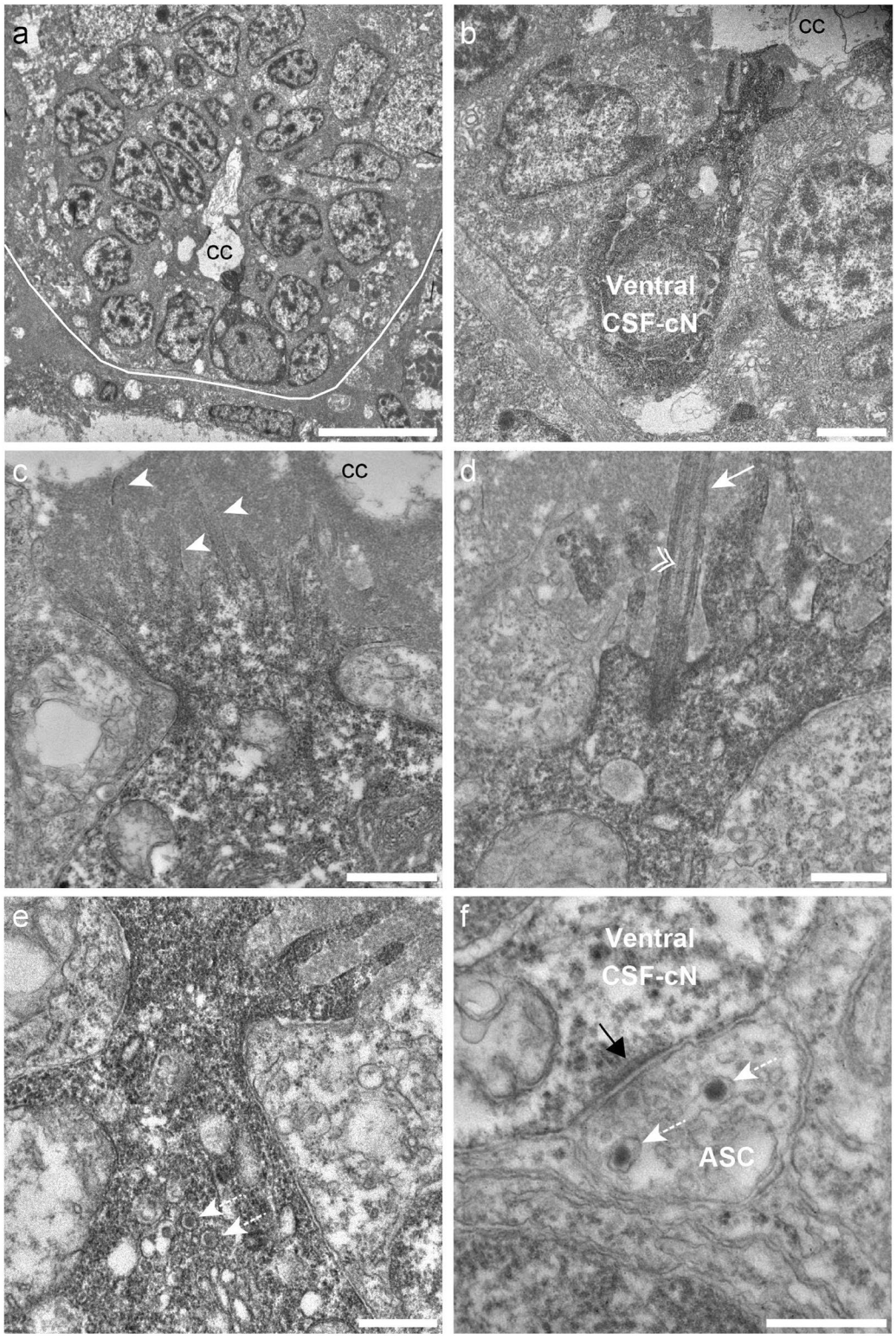

Figure 1. Ventral CSF-cNs exhibit an apical extension composed of microvilli and a kinocilium in the spinal cord. (**a**) Transverse section of the spinal cord showing restricted deposition of DAB in a ventral CSF-cN. (**b**) Overall view of a DAB^{+} ventral CSF-cN contacting the central canal (cc) and surrounded by ependymal cells. (**c**) Ventral CSF-cNs project at the apical pole an extension toward the central canal bearing several microvilli (arrowheads). (**d**) Within this extension is located a cilium (arrows) with two central microtubule along the axoneme (double arrowhead), suggesting a motile cilium. Large granular vesicles (LGV) are observed in the cytoplasm (**e**, dotted arrows) and axo-somatic synaptic contacts in the basal pole (**f**, ASC). Note the symmetry of the synaptic contact (black arrow) is reminiscent of an inhibitory synapse. Note the presence of LGV in the axon (**f**, dotted arrows). Scale bar = 10 μm (**a**), 2 μm (**b**), 1 μm (**c**), 500 nm (**d**,**e**) and 400 nm (**f**).

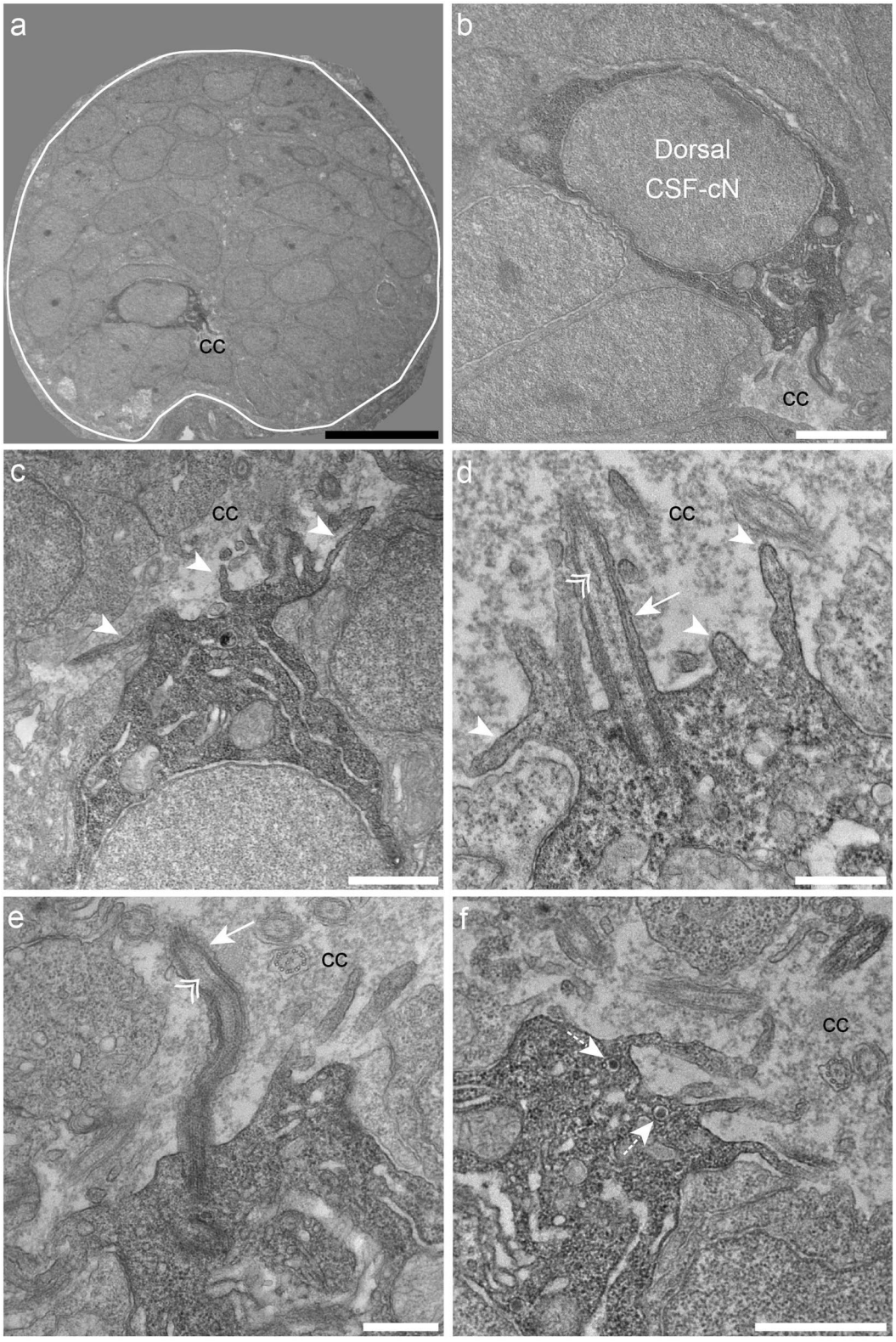

Figure 2. Dorsal spinal CSF-cNs also exhibit ultrastructural properties of sensory neurons. (**a**) Transverse section of the spinal cord showing restricted deposition of DAB in a dorsal CSF-cN. (**b**) Overall view of a DAB^{+} dorsal CSF-cN contacting the central canal (cc). (**c**,**d**) Dorsal CSF-cNs bear at the apical pole multiple microvilli (arrowheads). (**d**,**e**) In the apical pole is located a cilium (arrow) with two central microtubule singlets along the axoneme (double arrowhead), reminiscent of a motile cilium. (**f**) Dorsal CSF-cN also exhibit LGV distributed in the cytoplasm (dotted arrows). Scale bar = 10 μm (**a**), 2 μm (**b**), 1 μm (**c**,**f**) and 500 nm (**d**,**e**).

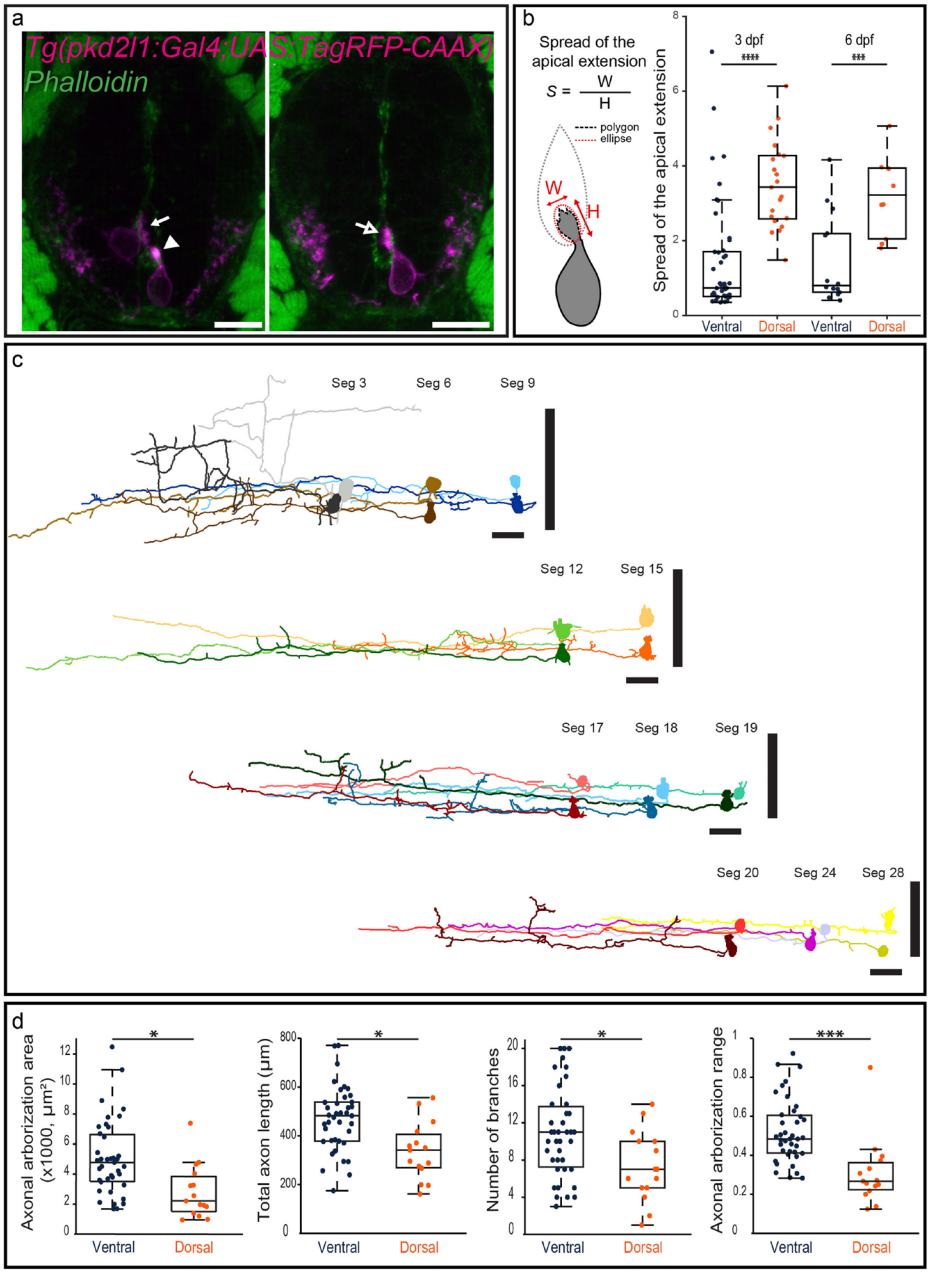

Figure 3. Morphological analysis of CSF-cNs reveals heterogeneous shapes of apical extension and axonal projections. (**a**) Transverse sections showing ventral and dorsal TagRFP-CAAX^{+} CSF-cNs (magenta) at 3 dpf reflecting the diversity of morphologies of the apical extension. The apical extension of all dorsal CSF-cNs spreads along the central canal border (arrow) while most ventral CSF-cNs (86.7%) form compact extensions (arrowhead). The small remaining subpopulation of ventral CSF-cNs exhibits the typical spread of dorsal apical extensions (arrow with empty head; Phalloidin staining, green). (**b**) Schematics of the analysis of the apical extension performed on each cell and statistical analysis comparing the size of the apical extension between ventral and dorsal CSF-cNs at 3 dpf (n = 45 versus 21) and 6 dpf (n = 14 versus 10). The apical extension of dorsal CSF-cNs extends more than for ventral CSF-cNs (two-sample t-tests, $p < 5 \cdot 10^{-7}$) and this difference persists at later stages (6 dpf, $p < 0.002$). (**c**) The reconstruction from dorsal (light shade) and ventral (dark shade) CSF-cNs from different segments (Seg) illustrates the diversity of axonal morphologies CSF-cNs between the two types along the spinal cord (n = 11 for each type). Vertical black bars represent the dorso-ventral limits of the spinal cord. Cells are positioned according to their dorso-ventral (D-V) position with dorsal edge set to 1 and ventral to 0. (**d**) Comparison of ventral and dorsal CSF-cNs for axonal arborization area, total axon length, number of branches and axonal arborization dorso-ventral range (n = 39 and 15 cells respectively). Ventral CSF-cNs have a wider axonal arborization ($p < 0.003$), a longer axon ($p = 0.0014$), reach more ventral domains of the spinal cord ($p < 9 \cdot 10^{-4}$), and cover a larger dorso-ventral (D-V) range ($p < 2 \cdot 10^{-4}$) with more axonal branches ($p < 0.02$). Two-sample t-tests were performed to compare the two populations. Scale bar = 10 µm (**a**) and 20 µm (**c**).

neurons and commissural primary ascending (CoPA) sensory interneurons within the escape circuit[43] as well as onto V0-v interneurons within the slow swimming circuit[15]. We investigated which CSF-cN type projects onto these targets using mosaic labeling in transgenic lines labeling CaP (*Tg*(*parg*^{mnet2}*-GFP*)[43, 44]), V0-v (*Tg*(*vglut2a*:*lox*:*DsRed*:*lox*:*GFP*)[15, 45]) or CoPA (*Tg*(*tbx16-GFP*)[43, 46]). We observed that only ventral CSF-cNs form the stereotypical basket structure around the soma of CaP motor neurons (Fig. 4a, n = 7 out of 8 ventral CSF-cNs found projecting onto CaP and 0 out of 5 dorsal CSF-cNs). In contrast, we found only dorsal CSF-cNs contacting ventrolateral glutamatergic cells, putatively V0-v based on their location and our previous findings[15, 47–49] (Fig. 4b, n = 3 out of 3 dorsal CSF-cNs and 0 out of 5 ventral CSF-cNs). Interestingly, we observed that both ventral and dorsal CSF-cNs project onto CoPA sensory interneurons (Fig. 4c,d, n = 4 dorsal and 5 ventral CSF-cNs). Altogether, our observations demonstrate a complex connectivity pattern from CSF-cNs onto their neuronal targets in the spinal cord. While some targets receive projections from both CSF-cN types (such as CoPA sensory interneurons), others seem to only receive inputs from either ventral (CaP motor neurons) or dorsal (ventrolateral glutamatergic neurons, most likely V0-v interneurons) CSF-cNs.

Investigation of secreted compounds expressed in dorsal and ventral CSF-cNs. We tested whether ventral and dorsal CSF-cNs differentially express secreted compounds previously reported in a restricted number of CSF-cNs, namely somatostatin[14, 21, 33, 34] and serotonin[35, 36]. By taking advantage of *pkd2l1* expression in CSF-cNs[13], we used the *Tg*(*pkd2l1*:*GCaMP5G*)*icm07* transgenic line to selectively target CSF-cNs[37]. We demonstrated the specificity of this line using fluorescent *in situ* hybridization (FISH) for *pkd2l1* mRNA coupled to GFP immunohistochemistry (IHC) to amplify the endogenous GCaMP5G signal from 24 hours post fertilization (hpf) to 5 dpf (Supplemental Fig. 5).

In zebrafish, somatostatin immunoreactivity has previously been reported[12], but 6 different paralogs exist (*sst1.1*, *sst1.2*, *sst2*, *sst3*, *sst5* and *sst6*)[50, 51]. Testing the expression of all of them, we only detected expression of *sst1.1* in CSF-cNs. Expression of *sst1.1* was observed only in dorsal CSF-cNs (Fig. 5a,b, arrows) in the rostral part of the spinal cord, from segment 1 to 13 at 24, 48, 72 hpf and in the adult spinal cord (data *not shown*). Since *sst1.1* had been reported as expressed transiently in motor neurons from 19 hpf until 55 hpf[52], we showed using FISH for *sst1.1* with GFP IHC in 24 hpf *Tg*(*mnx1*:*GFP*) embryos[53] that *sst1.1* expression was excluded from motor neurons (Fig. 5c). Altogether, our results show that *sst1.1* is expressed in dorsal CSF-cNs and absent in ventral ones at early stages and restricted as well to a subpopulation of CSF-cNs in the adult. Next, we tested whether zebrafish CSF-cNs were serotoninergic by performing double IHC for 5-HT and GFP on *Tg*(*pkd2l1*:*GCaMP5G*)*icm07* embryos and larvae from 24 hpf to 72 hpf. At 24 hpf, no 5-HT immunostaining was detected in the zebrafish spinal cord (*data not shown*). At 48 hpf, we detected 5-HT in ventral CSF-cNs (Fig. 5d, arrowheads) in the rostral part of the spinal cord (from segment 1 to 24). This expression was restricted to a subset of ventral CSF-cNs (Fig. 5d). The proportion of 5-HT^{+} CSF-cNs at 48 hpf decreased along the rostrocaudal axis of the spinal cord (segments 3 to 6: 88.6 ± 16.0%, 96 cells; segments 10 to 13: 73.2 ± 27.3%, 100 cells; segments 23 to 26: 31.2 ± 33.3%, 94 cells). At 3 dpf, although 5-HT was still expressed along the entire spinal cord in other cells, the staining was absent in CSF-cNs in the rostral spinal cord (Fig. 5e). In conclusion, dorsal CSF-cNs express *sst1.1* while a subpopulation of ventral CSF-cNs population is transiently serotoninergic. Hence, these two populations originating from different progenitor pools differentiate into distinct cell types expressing specific secreted compounds.

***pkd2l1* null mutation does not impact on the differentiation of spinal CSF-cNs.** We previously showed that the PKD2L1 channel is expressed in spinal CSF-cNs across multiple vertebrate species[13] and that the channel appears necessary to mediate detection of spinal bending by CSF-cNs in the larva[37]. In *pkd2l1* mutants, we observed defects in locomotion that we interpreted as being caused by the lack of sensory responses in CSF-cNs[37]. To strengthen the conclusions of this previous study, we sought to precisely assess whether CSF-cNs develop properly in the *pkd2l1* mutants. We found that in mutants, CSF-cNs were still GABAergic, ventral ones were still serotoninergic, that the number of CSF-cNs was not impacted, and that the morphology of their axonal projections was not different from WT (Supplemental Fig. 6). We also wanted to determine whether the functional connection between ventral CSF-cNs and CaPs[43, 54] was impacted and found that light-mediated activation of mutants CSF-cNs was still able to induce monosynaptic inhibitory postsynaptic currents in CaPs (Supplemental Fig. 7). Altogether, our results show that *pkd2l1* is not required for CSF-cN differentiation.

Discussion

Spinal CSF-cNs were previously shown to originate from distinct progenitor domains characterized by distinct pools of transcription factors in the embryo[26, 29, 30]. Here we demonstrate that these two domains give rise to two cell types of CSF-cNs with probably distinct functional properties at the larval stages (Supplemental Fig. 8). First, the morphology of these two cell types differs both at the apical extension level as well as at the axonal level. Furthermore, we show that these differences in axonal projections lead to differences in neuronal targets reached in the spinal cord. Second, our ultrastructure data indicate that both ventral and dorsal CSF-cNs bear dense granules under the apical extension, suggesting possible roles in release or uptake of compounds from the CSF. We show that ventral and dorsal populations express distinct secreted factors, in particular 5-HT and *sst1.1*, during development. Finally we show that Pkd2l1 is not necessary for the differentiation of CSF-cNs. Altogether, our results demonstrate that the two cell types of CSF-cNs previously identified with different developmental origins segregate into distinct populations bearing specific functional properties.

Due to their peculiar apical extension contacting the CSF, it had been hypothesized that CSF-cNs may release compounds into the CSF[7, 55]. The presence of large granular vesicles (LGV) within CSF-cNs in our EM data, combined with expression of *sst1.1* and 5-HT for dorsal and ventral CSF-cNs respectively, reinforces this hypothesis.

Previous works have shown that CSF-cNs are chemosensory[11, 24, 56, 57] as well as mechanosensory cells[37, 43, 58]. In zebrafish larvae, we previously showed that dorsal CSF-cNs respond to lateral bending of the spinal cord[37] while

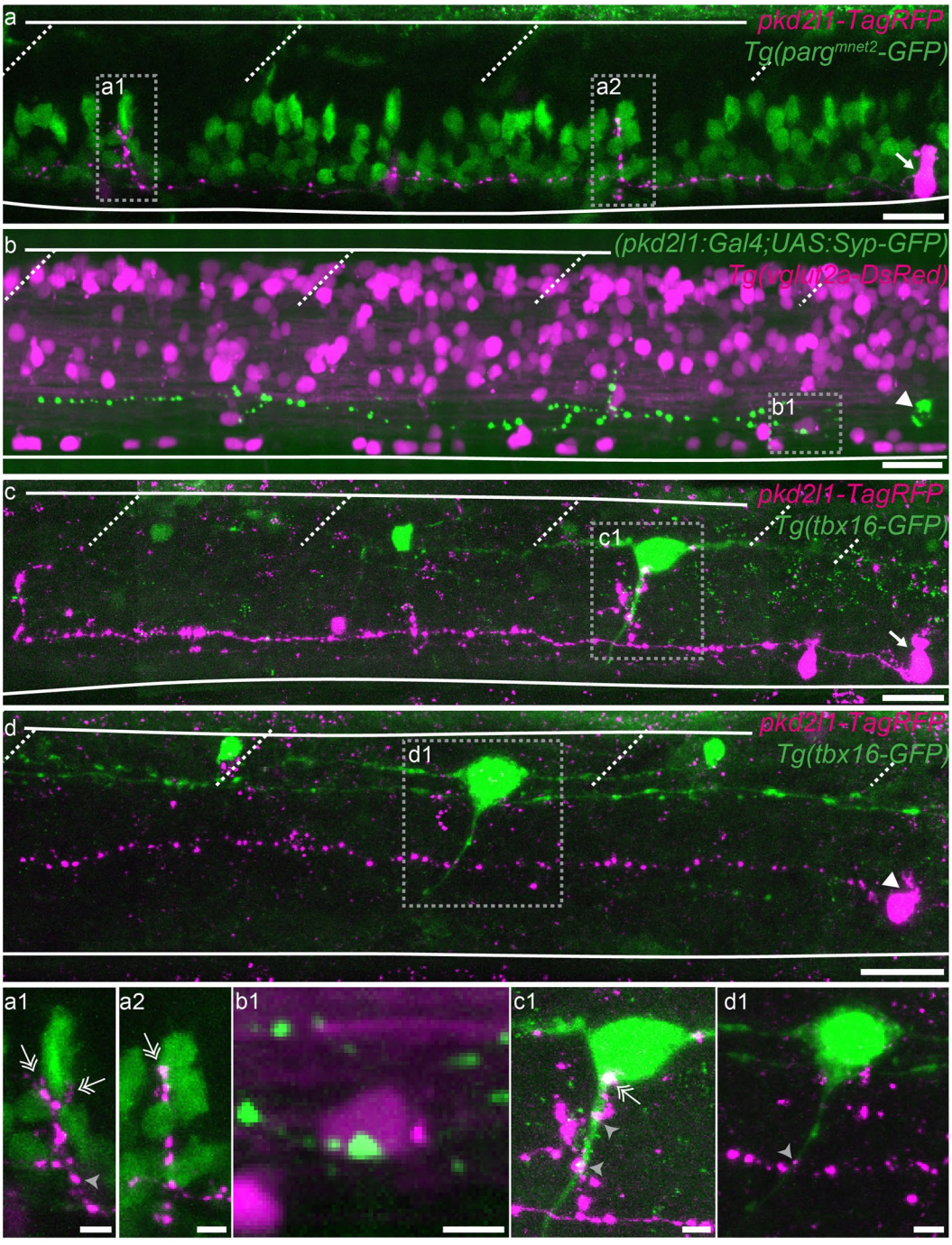

Figure 4. Ventral and dorsal CSF-cNs project onto distinct neuronal populations. (**a**–**d**) Z projection stacks showing contact from ventral and dorsal CSF-cNs onto different spinal targets. (**a**) Lateral view of a ventral CSF-cN (magenta, arrow) contacting 2 CaP motor neurons (identified based on their location within the segment) labelled in green in the *Tg*(*parg*^{mnet2}*-GFP*) transgenic line (**a1**,**a2**, double headed arrows). (**b**) Dorsal CSF-cN (green, arrowhead) contacting a putative V0-v interneuron (magenta, based on its dorso-ventral and lateral location) in the *Tg*(*vglut2a*:*DsRed*) transgenic line. (**c**,**d**) Ventral (**c**, arrow) and dorsal (**d**, arrowhead) CSF-cNs (magenta) contact CoPA sensory interneurons (green) labelled in the *Tg*(*tbx16-GFP*) transgenic line. Boxes with close-ups highlight contacts between the CSF-cN and its target. Scale bar = 20 µm (**a**–**d**) and 5 µm (**a1**–**d1**).

ventral CSF-cNs respond to longitudinal contractions[43]. The difference in shape of the apical extension between dorsal and ventral CSF-cNs may reflect a structural difference relevant for either their mechanosensory functions (direction of maximum sensitivity to bending of the tissue or CSF flow) or their secretory functions (with possibly larger surface area for dorsal CSF-cNs).

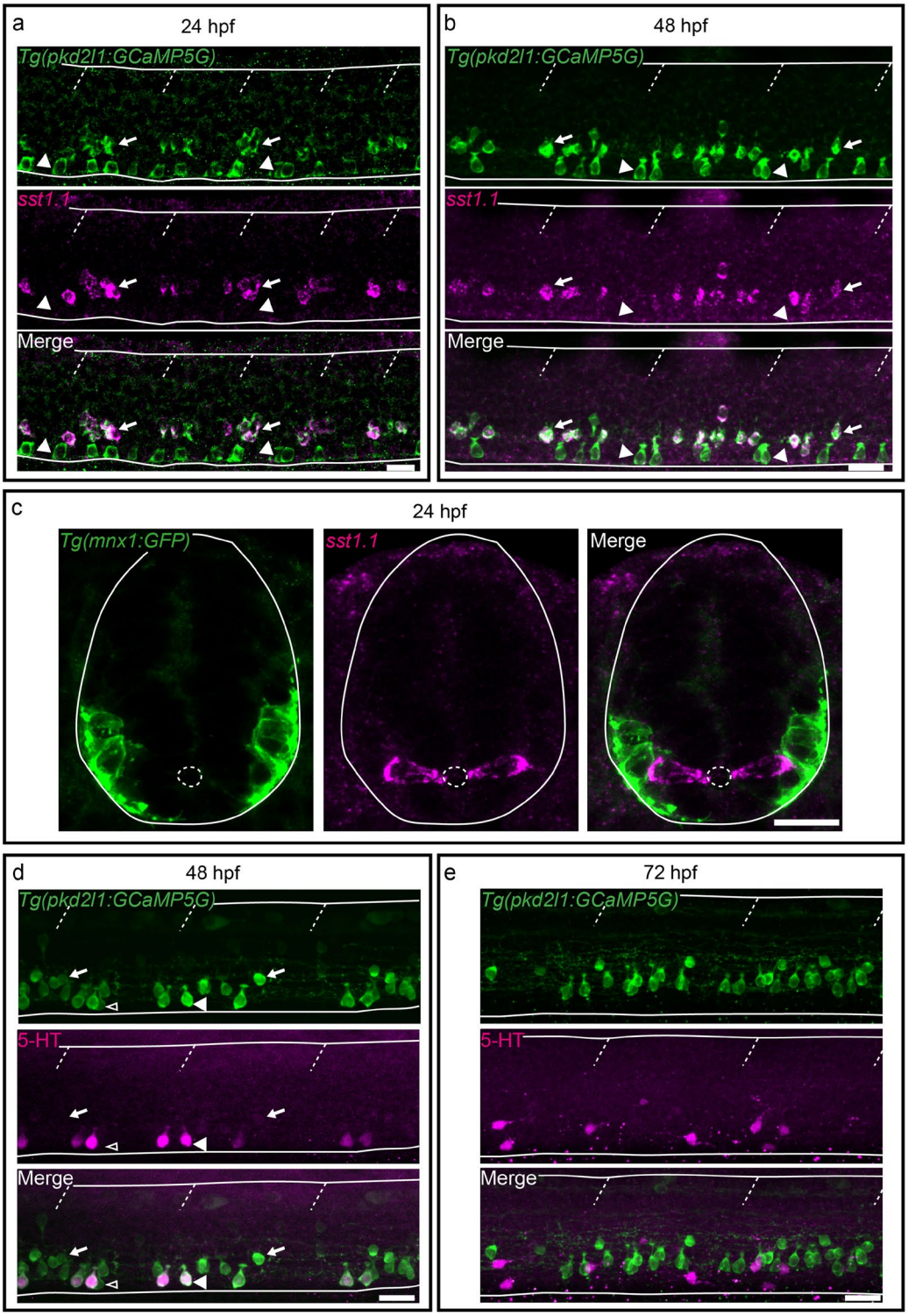

Figure 5. Secreted factors distinguish dorsal and ventral CSF-cNs: while dorsal express the somatostatin paralog *sst1.1*, ventral CSF-cNs express 5-HT. (**a**–**c**) Lateral views of the spinal cord show that *sst1.1* expression is restricted to dorsal CSF-cNs (arrows, FISH for *sst1.1* (magenta) coupled to GFP IHC (green) on *Tg*(*pkd2l1*:*GCaMP5G*)) (**a**,**b**) and *Tg*(*mnx1*:*GFP*) (**c**) embryos and larvae at 24 hpf (**a**,**c**) and 48 hpf (**b**). (**c**) Transverse sections show that *sst1.1* (magenta) is not expressed in motor neurons (green) as previously suggested (Devos *et al.*[52]). (**d**,**e**) IHC for 5-HT (magenta) and GFP (green) on *Tg*(*pkd2l1*:*GCaMP5G*) transgenic larvae at 48 hpf (**d**) and 72 hpf (**e**). (**d**) At 48 hpf, most ventral CSF-cNs express 5-HT (arrowhead, compared to negative cells shown with empty arrowhead). Note that dorsal CSF-cNs (arrows) are not labelled by 5-HT. (**e**) At 72 hpf, ventral CSF-cNs are not serotoninergic anymore in the rostral part of the spinal cord. Horizontal lines represent the limits of the spinal cord and slash dashed lines represent somite boundaries. Small dotted ellipses represent the limit of the central canal. Scale bars = 20 μm.

Transgenic/mutant	Labelling in the spinal cord	Original publication
Tg(pkd2l1:GCaMP5G)icm07	CSF-cNs	37
Tg(pkd2l1:GCaMP5G)icm07;pkd2l1^{icm02}	CSF-cNs	37
Tg(mnx1:GFP)	Motor neurons	53
Tg(pkd2l1:Gal4)icm10	CSF-cNs	15
Tg(UAS:TagRFP-CAAX;cmlc2:eGFP)icm22	Non applicable	This study
Tg(UAS:LifeAct-GFP;cryaa:V)icm28	Non applicable	This study
Tg(parg^{mnet2}*-GFP)*	Motor neurons	44
Tg(tbx16-GFP)	CoPAs	46
Tg(vglut2a:lox:DsRed:lox:GFP)	Glutamatergic interneurons	45

Table 1. Transgenic lines used in our study.

There are indications that spinal CSF-cNs harbor different morphologies in other species as well. In rat, spinal GABAergic CSF-cNs were first classified into three subtypes according to the shape of their soma[59]. Four morphological types of CSF-cNs were then described based on the shape of their soma, their axonal projection, and on the expression of the peptide Met-Enk-Arg-Gly-Leu[60]. These indications together with our data reveal a high level of heterogeneity among spinal CSF-cNs. Future studies will investigate the role of CSF-cN structural differences in sensory and secretory functions.

Using a single cell labelling approach, we show that ventral CSF-cNs have on average a longer and broader axonal arborization and cover a higher dorso-ventral spinal cord range with more axonal branches than dorsal CSF-cNs. These differences in axonal projections suggest the two CSF-cN populations might have distinct targets within the spinal cord. We had shown that CSF-cNs form active GABAergic synapses onto glutamatergic descending V0-v interneurons[15] as well as CaP primary motor neurons and CoPA sensory interneurons[43]. Here we show that only ventral CSF-cNs form the characteristic basket-like contact onto CaP soma while we only found dorsal CSF-cNs contacting ventrolateral glutamatergic neurons, most likely V0-v interneurons[47–49] previously shown to receive inputs from CSF-cNs[15]. Interestingly CoPA sensory interneurons received innervation from both dorsal and ventral CSF-cNs. Our results suggest that targets of the slow swimming circuits receive innervation from dorsal CSF-cNs while targets of the fast swimming circuit receive innervation from ventral CSF-cNs, and sensory interneurons involved in processing feedback receive innervation from both ventral and dorsal CSF-sNs. Further investigations will be necessary to establish whether other targets of the slow and fast swimming circuits follow the same dichotomy, receiving inputs from dorsal and ventral CSF-cNs respectively.

Multiple markers have been found in subsets of CSF-cNs across vertebrate species: somatostatin[12, 14, 21, 33, 34], dopamine[61–64] and serotonin[35, 36, 65]. The expression of most markers was reported in a restricted fraction of CSF-cNs. Here we tested whether some of these markers showed restricted expression patterns among CSF-cNs. We found that ventral CSF-cNs were at 48 hpf transiently serotoninergic as previously described in other species[35, 36, 65] in accordance with findings from Montgomery *et al.*[66], in zebrafish. In addition, we demonstrated that, even at 48 hpf, not all ventral CSF-cNs expressed 5-HT. This suggests that there may be different subtypes of ventral CSF-cNs based on 5-HT expression. Moreover, Montgomery *et al.*[66], also showed that the rate-limiting enzyme involved in 5-HT synthesis *tryptophan hydroxylase 1* a (*tph1a*)[67, 68] is expressed in the ventral spinal cord at 24 and 48 hpf suggesting that ventral CSF-cNs could constitute a transient source of serotonin at early stages. One possible explanation for the disappearance of 5-HT in ventral CSF-cNs at later stages could be the emergence of descending fibers from 5-HT^{+} neurons originating from the brainstem raphe nuclei from 48 hpf onwards[67]. 5-HT from descending fibers has been previously shown in mammals to suppress the monoaminergic expression of CSF-cNs[69–71]. The physiological relevance of the transient 5-HT expression among this ventral population of CSF-cNs remains to be elucidated.

Regarding the origin of somatostatin in zebrafish CSF-cNs, we found that among the six SST paralogs, *sst1.1* was the only one expressed. We demonstrated that the expression of this gene is specific and restricted to the dorsal population of CSF-cNs, identifying for the first time a specific marker of dorsal CSF-cNs. We also demonstrated that this peptide is excluded from motor neurons contrary to what previous studies suggested[52]. The physiological relevance of *sst1.1* expression by dorsal CSF-cNs is not known. In mammals and lamprey, it has been shown that somatostatin can reduce locomotor frequency[58, 72, 73]. The release of SST by dorsal CSF-cNs could impact the frequency of locomotor events along with the release of neuropeptides of the UII family, *urp1* and *urp2* by ventral CSF-cNs only[74] as previously suggested by the presence in coho salmon of a UII-like immunoreactive ventral population of CSF-cNs and a distinct somatostatinergic one[75]. Taken together, our results confirm that ventral and dorsal CSF-cNs express distinct peptides and neuromodulators. The transient nature of the expression of 5-HT suggest that it could have developmental roles to be further investigated.

Material and Methods

Animal care. Zebrafish (*Danio rerio*) adults and larvae were maintained and raised on a 14/10 hour light cycle. Fish lines used in this study are referenced in Table 1. Water was regulated at 28.5 °C, conductivity at 500 μS and pH at 7.4. All embryos and larvae under 6 dpf were anesthetized in 0.02% tricaine methane sulfonate (MS 222) (Sandoz, Levallois-Perret, France) and euthanized in 0.2% MS 222 prior to fixation. Experimental and animal protocols were approved by the Institut du Cerveau et de la Moelle Épinière in agreement with the French National Ethics Committee (Comité National de Réflexion Éthique sur l'Expérimentation Animale;

Ce5/2011/056) and European regulations.Genotype protocol for the *pkd2l1*^{icm02} mutants was described in ref. 37 (Böhm *et al*. 2016).

Generation of transgenic lines. In order to generate the *Tg*(*UAS*:*TagRFP-CAAX*;*cmlc2*:*eGFP*)*icm22* line, the TagRFP-CAAX sequence was amplified using a TagRFP-forward (5′-CCCGGGATCCACATGGTGTCTAAGGGCGAAG-3′) and reverse primer (5′-GATCGCGGCCGCTCAGGAGAGCACACACTTGCAGCTCATGCAGCCGGGGCCACTCTCATCAGGAGGGTTCAGCTTATTAAGTTTGTGCCC-3′) and inserted into the *pME-MCS* vector[76] via BamHI/NotI restriction digestion. The resulting *pME-TagRFP-CAAX* vector was recombined via a Gateway reaction (MultiSite Gateway Three-Fragment Vector Construction Kit) with *p5E-4nrUAS*[77], *p3E-pA* and *pDest-Tol2*; *cmlc2*:*eGFP*[76] resulting in (*p4nrUAS*:*TagRFP-CAAX-pA-Tol2*;*cmcl2*:*eGFP*). Using a similar approach, the *pME_LifeAct-GFP* plasmid was generated from the plasmid *pCS2_LifeAct-GFP* (kind gift from Nicolas David) using the SP6 promoter sequencing primer (5′-ATTTAGGTGACACTATAG-3′) and inserted into the pME_MCS vector via a BamHI/NotI restriction digestion. The final three-way gateway reaction used the *pME_LifeAct-GFP*, *pDest_cryaa*:*V* and *p5′E_polyA* plasmids to generate the (*UAS*:*LifeAct-GFP*;*cryaa*:*V*) construct. Microinjection of these plasmids was performed with Tol2 mRNA (25 ng/µl) following standard protocols. Transgenic founder fish *Tg*(*UAS*:*TagRFP-CAAX*;*cmlc2*:*eGFP*)*icm22* where screened based on GFP expression in the heart. These two lines were also screened based on transactivation of their respective transgene when crossed with various Gal4 lines.

Plasmid design. In order to investigate the CSF-cNs ultrastructure, we took advantage of the engineered peroxidase APEX2[78]. We generated a three-fragment Gateway recombining reaction (Invitrogen, Carlsbad, CA, USA) to design the (*UAS*:*APEX2-TagRFP*) construct. This plasmid was injected into single-cell stage *Tg*(*pkd2l1*:*Gal4*)*icm10* embryos at 60 ng/µl or co-injected with the (*pkd2l1*:*Gal4*)*icm10* construct into *Tg*(*pkd2l1*:*GaMP5G*)*icm07* singe-cell stage embryo. To generate the (*UAS*:*LifeAct-TagRFP*;*cryaa*:*C*) DNA construct, we extracted the coding sequence of the tagged protein LifeAct-TagRFP from the plasmid (*mTagRFP-T- LifeAct-7*) (Addgene #54586, kind gift from Michael Davidson) by PCR using a forward (5'-GGGGACAAGTTTGTACAAAAAAGCAGGCTAGATCTCTGCCACCATGGGCGTGGCCGACTTGATC-3') and a reverse (5'-GGGGACCACTTTGTACAAGAAAGCTGGGTACTAGTTTACTTGTACAGCTCGTCCATGCC-3') primer. LifeAct-TagRFP was then inserted into the plasmid *pDONR221* by a BP reaction to produce the *pME_LifeAct-TagRFP* plasmid and a three-way gateway reaction was performed using *pME_LifeAct-TagRFP*, *pDest_cryaa*:*C*, *p5′E_10XUAS* and *p3′E_polyA* plasmids to produce the (*UAS*:*LifeAct-TagRFP*;*cryaa*:*C*) construct.

Electron microscopy. To label CSF-cNs for electron microscopy, we followed the procedure described in refs 37, 78 and Supplemental Figs 2 and 3. 2.5 dpf larvae selected for TagRFP expression in CSF-cNs were primarily anaesthetized in 0.02% tricaine methane sulfonate (MS 222) then euthanized in 0.2% tricaine prior to fixation in 2% glutaraldehyde in 100 mM sodium cacodylate buffer pH 7.4 to which 2 mM of $CaCl_2$ was added for 45 min. Whole embryos were then rinsed in the same buffer 5 × 2 min each. Functional aldehyde excess was blocked by treating embryos for 5 min with 20 mM glycine in the sodium cacodylate buffer. Other rinses in buffer (5 × 2 min) were then carried out. The APEX2 peroxidase was further revealed in diaminobenzidine (DAB, 0.5 mg/ml) to which 10 mM hydrogen peroxide (30%) was added (see Lam *et al*.), in 100 mM cacodylate buffer. After 5 min, the reaction was stopped by rinsing embryos twice in cold buffer before post fixation in 2% osmium tetroxide (OsO_4) in the same buffer for 45 min. Embryos were then rinsed in cold distilled water, stained in 2% uranyl acetate in distilled water overnight in a cold chamber. Animals were returned to room temperature, rinsed in distilled water, then dehydrated in a graded series of ethanol, cleared in acetone, and embedded in epoxy resin (EMBed812, Electron Microscopy Science, France). Embryos were oriented coronally in resin molds cured at 60 °C for 48 hr. Whole embryos were imaged using a Leica DMRB microscope to assess the presence of DAB positive CSF-cNs and determine their location within the animals. Embryos were first cut in 1 µm semi-thin sections with an ultramicrotome (Ultracut E, Leica). Sections were picked up every µm, stained with toluidine blue. Semi-thin sectioning was performed until the first level of DAB^+ CSF-cN cell appears. Then, serial ultra-thin sections (~70 nm thick) were collected onto copper grids (about 8 sections per grid). 12 ventral CSF-cNs, and 3 dorsal CSF-cNs were analyzed. They were contrasted in urany-less solution (Delta Microscopies, France) for 1–2 min, rinsed in distilled water, dried for at least 1 hr. Observations were made with an Hitachi HT 7700 electron microscope operating at 70 kV. Electron micrographs from DAB^+ CSF-cNs were taken at low (×6200), medium (×22,000) and high (×53,000) magnifications, using an integrated AMT XR41-B camera (2048 × 2048 pixels). In all the images displayed, dorsal is up and rostral is left.

Analysis of the apical dendritic extension of CSF-cNs. To image the apical dendritic extension at a high resolution, we used different labeling strategies relying on transverse sections of the spinal cord. At 3 dpf, we used the stable *Tg*(*pkd2l1*:*Gal4*;*UAS*:*TagRFP-CAAX*;*cmlc2*:*eGFP*) transgenic line with membrane TagRFP and the transient expression of (*pkd2l1*:*Gal4*)[15] and (*UAS*:*LifeAct-TagRFP*;*cryaa*:*C*) DNA constructs injected into *Tg*(*pkd2l1*:*GCaMP5*)*icm07* eggs at the one cell stage to label F-actin with LifeAct[79]. At 6 dpf, we took advantage of the stable *Tg*(*pkd2l1*:*Gal4*;*UAS*:*LifeAct-GFP*;*cryaa*:*V*)*icm28* line. 3 and 6 dpf larvae were screened for expression in CSF-cNs and fixed using 4% paraformaldehyde (PFA) during 4 hours at 4 °C and immunostained as described below. We sliced 50 µm-thick transverse sections on larvae mounted in 3% low melting point agarose using a vibratome (HM 650 V Microtome, Thermo Scientific). For each cell, Z stacks (step size 0.25 µm) were acquired to image the entire apical extension and maximum projection was performed in Fiji[80]. The shape of the apical extension (S) was calculated as the ratio of the width (W, basal extension along the central canal) over the height (H, vertical extension within the central canal). W and H were extracted by drawing a polygon around the apical

extension using the polygon tool in Fiji and estimated by the parallel and perpendicular axis, respectively, of the best fitting ellipse (Fig. 4b).

Single cell labeling. To assess whether *pkd2l1* mutation led to a disruption of CSF-cN axonal refinement, we injected at 25 ng/µl the (*pkd2l1-TagRFP*) construct generated with a three-fragment Gateway recombineering reaction into single-cell stage embryos from *pkd2l1*$^{icm02/+}$ incrosses (see ref. 15). 3 dpf larvae selected for single CSF-cN expression were fixed with 4% PFA for 3 hours and immunostained following standard procedures. Genotyping of the larvae was performed after immunostaining. To assess the connectivity of ventral and dorsal CSF-cNs, the same procedure was followed when the (*pkd2l1-TagRFP*) construct has been injected in the *Tg*(*par g*^{mnet2}*-GFP*)[44] and *Tg*(*tbx16-GFP*)[46] *lines* and the (*pkd2l1*:*Gal4*) *with* (*UAS*:*synaptophysin-GFP*)[81] constructs in the *Tg*(*vglut2a.lox-DsRed-lox-GFP*)*line*[45]. Some of these animals have been imaged live.

Analysis of the axonal arborization of isolated CSF-cNs. To label and trace individual CSF-cNs, we followed the same procedure as described in ref. 15, in Supplemental Information and in Supplemental Fig. 4.

Fluorescent *in situ* (FISH). The *pkd2l1* ISH probe was generated as previously described[13]. The *sst1.1* plasmid originates from the Argenton lab, Padova, Italy[52,82]. *pkd2l1* and *sst1.1* plasmids were respectively linearized with NotI and SalI. Digoxigenin (DIG)- and fluorescein (Fluo)-labeled probes were synthesized using SP6 RNA polymerase with the RNA Labeling Kit (Roche Applied Science, Basel, Switzerland) to generate both *pkd2l1* and *sst1.1* antisense probes. All probes were purified using the mini Quick Spin RNA Column (Roche, Basel, Switzerland). Whole-mount ISH were performed as previously described[13,83] on embryos or larvae fixed in 4% PFA in phosphate buffered saline (PBS) overnight at 4 °C.

Immunohistochemistry (IHC). Procedures for IHC were described in Supplemental Information.

FISH coupled to IHC. Procedures were described in ref. 13. Briefly, *pkd2l1* and *sst1.1* FISH were performed prior to IHC of green fluorescent protein (GFP): embryos and larvae were washed and immunostained with the chicken anti-GFP antibody (1:500 dilution, Abcam ab13970, Cambridge, UK) overnight at 4 °C, and then incubated with the corresponding Alexa-conjugated secondary antibodies IgG (1:500, Invitrogen A11039, Carlsbad, CA, USA) combined with DAPI (2.5 µg/mL, Invitrogen D3571, Carlsbad, CA, USA).

Cell counting. To compare the density of markers investigated, we systematically imaged three regions along the rostrocaudal axis of the fish: segments 3–6 (referred as rostral), 10–13 (referred as middle and displayed in all Figures) and 23–26 (referred as caudal).

Imaging. Images were acquired using an Olympus FV1000 confocal microscope equipped with a 20 and 40x water and 60X oil immersion objectives using the 405, 473 and 543 nm laser lines or using an upright microscope (Examiner Z1, Zeiss) equipped with a spinning disk head (CSU-X1, Yokogawa) and a modular laser light source (LasterStack, 3i Intelligent Imaging Innovations). To determine the overlap of GFP in the *Tg*(*pkd2l1*:*GCaMP5G*)*icm07* transgenic embryos and larvae with *pkd2l1*, *sst1.1* FISH or GABA and 5-HT IHC, fish were mounted laterally in 1, 5% agarose covered of Vectashield Mounting Medium (Vectorlabs, CA, USA). To analyze apical extensions, slices were transferred into Vectashield mounting medium as well (Vectorlab, CA, USA).

Electrophysiology and optogenetic stimulation. Procedures for optogenetic stimulation of CSF-cNs and electrophysiological recordings of CaP motor neurons are described in Supplemental Information and Supplemental Fig. 7.

Statistics. We used Student's t-tests for the morphological comparison of ventral versus dorsal CSF-cNs in WT and *pkd2l1*$^{icm02/icm02}$ mutants and two-way ANOVAs to test the interaction between the genotypes and the cells investigated. The level of significance was $p < 0.05$ for all datasets. p values are represented as the following: (*)$p < 0.05$; (***)$p < 0.001$; (****)$p < 0.0001$.

References

1. Iliff, J. J. *et al.* A paravascular pathway facilitates CSF flow through the brain parenchyma and the clearance of interstitial solutes, including amyloid beta. *Sci Transl Med* **4**, 147ra111, doi:10.1126/scitranslmed.30037484/147/147ra111 (2012).
2. Pappenheimer, J. R., Miller, T. B. & Goodrich, C. A. Sleep-promoting effects of cerebrospinal fluid from sleep-deprived goats. *Proc Natl Acad Sci USA* **58**, 513–517 (1967).
3. Martin, F. H., Seoane, J. R. & Baile, C. A. Feeding in satiated sheep elicited by intraventricular injections of CSF from fasted sheep. *Life Sci* **13**, 177–184 (1973).
4. Lerner, R. A. *et al.* Cerebrodiene: a brain lipid isolated from sleep-deprived cats. *Proc Natl Acad Sci USA* **91**, 9505–9508 (1994).
5. Nishino, S. *et al.* Low cerebrospinal fluid hypocretin (Orexin) and altered energy homeostasis in human narcolepsy. *Ann Neurol* **50**, 381–388 (2001).
6. Xie, L. *et al.* Sleep drives metabolite clearance from the adult brain. *Science* **342**, 373–377, doi:10.1126/science.1241224342/6156/373 (2013).
7. Vigh, B., Vigh-Teichmann, I. & Aros, B. Special dendritic and axonal endings formed by the cerebrospinal fluid contacting neurons of the spinal cord. *Cell Tissue Res* **183**, 541–552 (1977).
8. Vigh, B. & Vigh-Teichmann, I. Actual problems of the cerebrospinal fluid-contacting neurons. *Microsc Res Tech* **41**, 57–83, doi:10.1002/(SICI)1097-0029(19980401)41:1<57::AID-JEMT6>3.0.CO;2-R (1998).
9. Kolmer, W. Das "Sagittalorgan" der Wirbeltiere. *Zeitschrift für Anatomie und Entwicklungsgeschichte* **60**, 652–717 (1921).
10. Agduhr, E. Über ein zentrales Sinnesorgan (?) bei den Vertebraten. *Zeitschrift für Anatomie und Entwicklungsgeschichte* **66**, 223–360 (1922).

11. Huang, A. L. *et al.* The cells and logic for mammalian sour taste detection. *Nature* **442**, 934–938, doi:10.1038/nature05084 (2006).
12. Wyart, C. *et al.* Optogenetic dissection of a behavioural module in the vertebrate spinal cord. *Nature* **461**, 407–410, doi:10.1038/nature08323nature08323 (2009).
13. Djenoune, L. *et al.* Investigation of spinal cerebrospinal fluid-contacting neurons expressing PKD2L1: evidence for a conserved system from fish to primates. *Front Neuroanat* **8**, 26, doi:10.3389/fnana.2014.00026 (2014).
14. Jalalvand, E., Robertson, B., Wallen, P., Hill, R. H. & Grillner, S. Laterally projecting cerebrospinal fluid-contacting cells in the lamprey spinal cord are of two distinct types. *J Comp Neurol* **522**, Spc1, doi:10.1002/cne.23584 (2014).
15. Fidelin, K. *et al.* State-Dependent Modulation of Locomotion by GABAergic Spinal Sensory Neurons. *Curr Biol* **25**, 3035–3047, doi:10.1016/j.cub.2015.09.070 (2015).
16. LaMotte, C. C. Vasoactive intestinal polypeptide cerebrospinal fluid-contacting neurons of the monkey and cat spinal central canal. *J Comp Neurol* **258**, 527–541, doi:10.1002/cne.902580405 (1987).
17. Stoeckel, M. E. *et al.* Cerebrospinal fluid-contacting neurons in the rat spinal cord, a gamma-aminobutyric acidergic system expressing the P2X2 subunit of purinergic receptors, PSA-NCAM, and GAP-43 immunoreactivities: light and electron microscopic study. *J Comp Neurol* **457**, 159–174, doi:10.1002/cne.10565 (2003).
18. Marichal, N., Garcia, G., Radmilovich, M., Trujillo-Cenoz, O. & Russo, R. E. Enigmatic central canal contacting cells: immature neurons in "standby mode"? *J Neurosci* **29**, 10010–10024, doi:10.1523/JNEUROSCI.6183-08.200929/32/10010 (2009).
19. Christenson, J., Bongianni, F., Grillner, S. & Hokfelt, T. Putative GABAergic input to axons of spinal interneurons and primary sensory neurons in the lamprey spinal cord as shown by intracellular Lucifer yellow and GABA immunohistochemistry. *Brain Res* **538**, 313–318 (1991).
20. Megias, M., Alvarez-Otero, R. & Pombal, M. A. Calbindin and calretinin immunoreactivities identify different types of neurons in the adult lamprey spinal cord. *J Comp Neurol* **455**, 72–85, doi:10.1002/cne.10473 (2003).
21. Christenson, J., Alford, S., Grillner, S. & Hokfelt, T. Co-localized GABA and somatostatin use different ionic mechanisms to hyperpolarize target neurons in the lamprey spinal cord. *Neurosci Lett* **134**, 93-97, doi:0304-3940(91)90516-V (1991).
22. Delmas, P. Polycystins: from mechanosensation to gene regulation. *Cell* **118**, 145–148, doi:10.1016/j.cell.2004.07.007S0092867404006671 (2004).
23. Orts-Del'immagine, A. *et al.* Properties of subependymal cerebrospinal fluid contacting neurones in the dorsal vagal complex of the mouse brainstem. *J Physiol* **590**, 3719–3741, doi:10.1113/jphysiol.2012.227959jphysiol.2012.227959 (2012).
24. Orts Del'Immagine, A. *et al.* A single polycystic kidney disease 2-like 1 channel opening acts as a spike generator in cerebrospinal fluid-contacting neurons of adult mouse brainstem. *Neuropharmacology*, doi:10.1016/j.neuropharm.2015.07.030 (2015).
25. Orts-Del'immagine, A. *et al.* Morphology, Distribution and Phenotype of Polycystin Kidney Disease 2-like 1-Positive Cerebrospinal Fluid Contacting Neurons in The Brainstem of Adult Mice. *PLoS One* **9**, e87748, doi:10.1371/journal.pone.0087748PONE-D-13-31038 (2014).
26. Petracca, Y. L. *et al.* The late and dual origin of cerebrospinal fluid-contacting neurons in the mouse spinal cord. *Development* **143**, 880–891, doi:10.1242/dev.129254 (2016).
27. Ishimaru, Y. *et al.* Transient receptor potential family members PKD1L3 and PKD2L1 form a candidate sour taste receptor. *Proc Natl Acad Sci USA* **103**, 12569–12574, doi:10.1073/pnas.0602702103 (2006).
28. Shimizu, T., Janssens, A., Voets, T. & Nilius, B. Regulation of the murine TRPP3 channel by voltage, pH, and changes in cell volume. *Pflugers Arch* **457**, 795–807, doi:10.1007/s00424-008-0558-6 (2009).
29. Park, H. C., Shin, J. & Appel, B. Spatial and temporal regulation of ventral spinal cord precursor specification by Hedgehog signaling. *Development* **131**, 5959–5969, doi:10.1242/dev.01456 (2004).
30. Yang, L., Rastegar, S. & Strahle, U. Regulatory interactions specifying Kolmer-Agduhr interneurons. *Development* **137**, 2713–2722, doi:10.1242/dev.048470dev.048470 (2010).
31. England, S., Batista, M. F., Mich, J. K., Chen, J. K. & Lewis, K. E. Roles of Hedgehog pathway components and retinoic acid signalling in specifying zebrafish ventral spinal cord neurons. *Development* **138**, 5121–5134, doi:10.1242/dev.066159138/23/5121 (2011).
32. Huang, P., Xiong, F., Megason, S. G. & Schier, A. F. Attenuation of Notch and Hedgehog signaling is required for fate specification in the spinal cord. *PLoS Genet* **8**, e1002762, doi:10.1371/journal.pgen.1002762PGENETICS-D-11-02695 (2012).
33. Buchanan, J. T., Brodin, L., Hokfelt, T., Van Dongen, P. A. & Grillner, S. Survey of neuropeptide-like immunoreactivity in the lamprey spinal cord. *Brain Res* **408**, 299–302, doi:0006-8993(87)90392-1 (1987).
34. Lopez, J. M. *et al.* Distribution of somatostatin-like immunoreactivity in the brain of the caecilian Dermophis mexicanus (Amphibia: Gymnophiona): comparative aspects in amphibians. *J Comp Neurol* **501**, 413–430, doi:10.1002/cne.21244 (2007).
35. Sims, T. J. The development of monamine-containing neurons in the brain and spinal cord of the salamander, Ambystoma mexicanum. *J Comp Neurol* **173**, 319–336, doi:10.1002/cne.901730208 (1977).
36. Chiba, A. & Oka, S. Serotonin-immunoreactive structures in the central nervous system of the garfish Lepisosteus productus (Semionotiformes, Osteichthyes). *Neurosci Lett* **261**, 73–76, doi:S0304-3940(98)01011-8 (1999).
37. Böhm, U. L. *et al.* CSF-contacting neurons regulate locomotion by relaying mechanical stimuli to spinal circuits. *Nat Commun* **7**, 10866, doi:10.1038/ncomms10866 (2016).
38. Flock, A. & Duvall, A. J. 3rd The Ultrastructure of the Kinocilium of the Sensory Cells in the Inner Ear and Lateral Line Organs. *J Cell Biol* **25**, 1–8 (1965).
39. Kindt, K. S., Finch, G. & Nicolson, T. Kinocilia mediate mechanosensitivity in developing zebrafish hair cells. *Dev Cell* **23**, 329–341, doi:10.1016/j.devcel.2012.05.022S1534-5807(12)00249-3 (2012).
40. DeFelipe, J. Types of neurons, synaptic connections and chemical characteristics of cells immunoreactive for calbindin-D28K, parvalbumin and calretinin in the neocortex. *J Chem Neuroanat* **14**, 1–19, doi:S0891061897100138 (1997).
41. Fiala, J. C., Feinberg, M., Popov, V. & Harris, K. M. Synaptogenesis via dendritic filopodia in developing hippocampal area CA1. *J Neurosci* **18**, 8900–8911 (1998).
42. Megias, M., Emri, Z., Freund, T. F. & Gulyas, A. I. Total number and distribution of inhibitory and excitatory synapses on hippocampal CA1 pyramidal cells. *Neuroscience* **102**, 527–540, doi:S0306-4522(00)00496-6 (2001).
43. Hubbard, J. M. *et al.* Intraspinal Sensory Neurons Provide Powerful Inhibition to Motor Circuits Ensuring Postural Control during Locomotion. *Curr Biol* **26**, 2841–2853, doi:10.1016/j.cub.2016.08.026 (2016).
44. Balciunas, D. *et al.* Enhancer trapping in zebrafish using the Sleeping Beauty transposon. *BMC Genomics* **5**, 62, doi:10.1186/1471-2164-5-62 (2004).
45. Koyama, M., Kinkhabwala, A., Satou, C., Higashijima, S. & Fetcho, J. Mapping a sensory-motor network onto a structural and functional ground plan in the hindbrain. *Proc Natl Acad Sci USA* **108**, 1170–1175, doi:10.1073/pnas.1012189108 (2011).
46. Wells, S., Nornes, S. & Lardelli, M. Transgenic zebrafish recapitulating tbx16 gene early developmental expression. *PLoS One* **6**, e21559, doi:10.1371/journal.pone.0021559 (2011).
47. Hale, M. E., Ritter, D. A. & Fetcho, J. R. A confocal study of spinal interneurons in living larval zebrafish. *J Comp Neurol* **437**, 1–16 (2001).
48. McLean, D. L., Fan, J., Higashijima, S., Hale, M. E. & Fetcho, J. R. A topographic map of recruitment in spinal cord. *Nature* **446**, 71–75, doi:10.1038/nature05588 (2007).
49. Satou, C., Kimura, Y. & Higashijima, S. Generation of multiple classes of V0 neurons in zebrafish spinal cord: progenitor heterogeneity and temporal control of neuronal diversity. *J Neurosci* **32**, 1771–1783, doi:10.1523/JNEUROSCI.5500-11.2012 (2012).

50. Tostivint, H., Lihrmann, I. & Vaudry, H. New insight into the molecular evolution of the somatostatin family. *Mol Cell Endocrinol* **286**, 5–17, doi:10.1016/j.mce.2008.02.029S0303-7207(08)00115-9 (2008).
51. Tostivint, H., Quan, F. B., Bougerol, M., Kenigfest, N. B. & Lihrmann, I. Impact of gene/genome duplications on the evolution of the urotensin II and somatostatin families. *Gen Comp Endocrinol* **188**, 110–117, doi:10.1016/j.ygcen.2012.12.015S0016-6480(13)00005-1 (2013).
52. Devos, N. *et al.* Differential expression of two somatostatin genes during zebrafish embryonic development. *Mech Dev* **115**, 133–137, doi:S0925477302000825 (2002).
53. Flanagan-Steet, H., Fox, M. A., Meyer, D. & Sanes, J. R. Neuromuscular synapses can form *in vivo* by incorporation of initially aneural postsynaptic specializations. *Development* **132**, 4471–4481, doi:10.1242/dev.02044 (2005).
54. Sternberg, J. R. *et al.* Optimization of a Neurotoxin to Investigate the Contribution of Excitatory Interneurons to Speed Modulation *In Vivo*. *Curr Biol* **26**, 2319–2328, doi:10.1016/j.cub.2016.06.037 (2016).
55. Vigh, B. & Vigh-Teichmann, I. Structure of the medullo-spinal liquor-contacting neuronal system. *Acta Biol Acad Sci Hung* **22**, 227–243 (1971).
56. Bushman, J. D., Ye, W. & Liman, E. R. A proton current associated with sour taste: distribution and functional properties. *FASEB J* **29**, 3014–3026, doi:10.1096/fj.14-265694fj.14-265694 (2015).
57. Jalalvand, E., Robertson, B., Tostivint, H., Wallen, P. & Grillner, S. The Spinal Cord Has an Intrinsic System for the Control of pH. *Curr Biol* **26**, 1346–1351, doi:10.1016/j.cub.2016.03.048 (2016).
58. Jalalvand, E., Robertson, B., Wallen, P. & Grillner, S. Ciliated neurons lining the central canal sense both fluid movement and pH through ASIC3. *Nat Commun* **7**, 10002, doi:10.1038/ncomms10002 (2016).
59. Barber, R. P., Vaughn, J. E. & Roberts, E. The cytoarchitecture of GABAergic neurons in rat spinal cord. *Brain Res* **238**, 305–328, doi:0006-8993(82)90107-X (1982).
60. Shimosegawa, T. *et al.* An immunohistochemical study of methionine-enkephalin-Arg6-Gly7-Leu8-like immunoreactivity-containing liquor-contacting neurons (LCNs) in the rat spinal cord. *Brain Res* **379**, 1–9, doi:0006-8993(86)90249-0 (1986).
61. Barreiro-Iglesias, A., Villar-Cervino, V., Anadon, R. & Rodicio, M. C. Descending brain-spinal cord projections in a primitive vertebrate, the lamprey: cerebrospinal fluid-contacting and dopaminergic neurons. *J Comp Neurol* **511**, 711–723, doi:10.1002/cne.21863 (2008).
62. Rodicio, M. C., Villar-Cervino, V., Barreiro-Iglesias, A. & Anadon, R. Colocalization of dopamine and GABA in spinal cord neurones in the sea lamprey. *Brain Res Bull* **76**, 45–49, doi:10.1016/j.brainresbull.2007.10.062S0361-9230(07)00399-1 (2008).
63. Roberts, B. L., Maslam, S., Scholten, G. & Smit, W. Dopaminergic and GABAergic cerebrospinal fluid-contacting neurons along the central canal of the spinal cord of the eel and trout. *J Comp Neurol* **354**, 423–437, doi:10.1002/cne.903540310 (1995).
64. Acerbo, M. J., Hellmann, B. & Gunturkun, O. Catecholaminergic and dopamine-containing neurons in the spinal cord of pigeons: an immunohistochemical study. *J Chem Neuroanat* **25**, 19–27, doi:S0891061802000728 (2003).
65. Parent, A. & Northcutt, R. G. The monoamine-containing neurons in the brain of the garfish, Lepisosteus osseus. *Brain Res Bull* **9**, 189–204 (1982).
66. Montgomery, J. E., Wiggin, T. D., Rivera-Perez, L. M., Lillesaar, C. & Masino, M. A. Intraspinal serotonergic neurons consist of two, temporally distinct populations in developing zebrafish. *Dev Neurobiol* **76**, 673–687, doi:10.1002/dneu.22352 (2016).
67. Bellipanni, G., Rink, E. & Bally-Cuif, L. Cloning of two tryptophan hydroxylase genes expressed in the diencephalon of the developing zebrafish brain. *Mech Dev* **119** Suppl 1, S215–220, doi:S0925477303001199 (2002).
68. Teraoka, H. *et al.* Hedgehog and Fgf signaling pathways regulate the development of tphR-expressing serotonergic raphe neurons in zebrafish embryos. *J Neurobiol* **60**, 275–288, doi:10.1002/neu.20023 (2004).
69. Branchereau, P., Chapron, J. & Meyrand, P. Descending 5-hydroxytryptamine raphe inputs repress the expression of serotonergic neurons and slow the maturation of inhibitory systems in mouse embryonic spinal cord. *J Neurosci* **22**, 2598–2606, doi:20026199 (2002).
70. Allain, A. E., Segu, L., Meyrand, P. & Branchereau, P. Serotonin controls the maturation of the GABA phenotype in the ventral spinal cord via 5-HT1b receptors. *Ann N Y Acad Sci* **1198**, 208–219, doi:10.1111/j.1749-6632.2010.05433.x (2010).
71. Wienecke, J. *et al.* Spinal cord injury enables aromatic L-amino acid decarboxylase cells to synthesize monoamines. *J Neurosci* **34**, 11984–12000, doi:10.1523/JNEUROSCI.3838-13.2014 (2014).
72. Barriere, G., Bertrand, S. & Cazalets, J. R. Peptidergic neuromodulation of the lumbar locomotor network in the neonatal rat spinal cord. *Peptides* **26**, 277–286, doi:10.1016/j.peptides.2004.09.002 (2005).
73. Miles, G. B. & Sillar, K. T. Neuromodulation of vertebrate locomotor control networks. *Physiology (Bethesda)* **26**, 393–411, doi:10.1152/physiol.00013.201126/6/393 (2011).
74. Quan, F. B. *et al.* Comparative distribution and *in vitro* activities of the urotensin II-related peptides URP1 and URP2 in zebrafish: evidence for their colocalization in spinal cerebrospinal fluid-contacting neurons. *PLoS One* **10**, e0119290, doi:10.1371/journal.pone.0119290PONE-D-14-36037 (2015).
75. Yulis, C. R. & Lederis, K. Relationship between urotensin II- and somatostatin-immunoreactive spinal cord neurons of Catostomus commersoni and Oncorhynchus kisutch (Teleostei). *Cell Tissue Res* **254**, 539–542 (1988).
76. Kwan, K. M. *et al.* The Tol2kit: a multisite gateway-based construction kit for Tol2 transposon transgenesis constructs. *Dev Dyn* **236**, 3088–3099, doi:10.1002/dvdy.21343 (2007).
77. Auer, T. O. *et al.* Deletion of a kinesin I motor unmasks a mechanism of homeostatic branching control by neurotrophin-3. *Elife* **4**, 10.7554/eLife.05061 (2015).
78. Lam, S. S. *et al.* Directed evolution of APEX2 for electron microscopy and proximity labeling. *Nat Methods* **12**, 51–54, doi:10.1038/nmeth.3179nmeth.3179 (2015).
79. Riedl, J. *et al.* Lifeact: a versatile marker to visualize F-actin. *Nat Methods* **5**, 605–607, doi:10.1038/nmeth.1220 (2008).
80. Schindelin, J. *et al.* Fiji: an open-source platform for biological-image analysis. *Nat Methods* **9**, 676–682, doi:10.1038/nmeth.2019nmeth.2019 (2012).
81. Meyer, M. P. & Smith, S. J. Evidence from *in vivo* imaging that synaptogenesis guides the growth and branching of axonal arbors by two distinct mechanisms. *J Neurosci* **26**, 3604–3614, doi:10.1523/JNEUROSCI.0223-06.2006 (2006).
82. Argenton, F., Zecchin, E. & Bortolussi, M. Early appearance of pancreatic hormone-expressing cells in the zebrafish embryo. *Mech Dev* **87**, 217–221, doi:S0925-4773(99)00151-3 (1999).
83. Parmentier, C. *et al.* Occurrence of two distinct urotensin II-related peptides in zebrafish provides new insight into the evolutionary history of the urotensin II gene family. *Endocrinology* **152**, 2330–2341, doi:10.1210/en.2010-1500en.2010-1500 (2011).

Acknowledgements

We thank Natalia Maties and Bogdan Buzurin from Animalliance for expert fish care. We thank Prof. Hervé Tostivint for precious feedback regarding the somatostatin experiments. We thank Déborah Delpeuch for help with genotyping and Sophie Nunes Figueiredo for technical assistance. We thank Peter Steenbergen, Dr Soojin Ryu, Freiburg University, Germany and Dr Heiko Loehr, University of Cologne, Germany for providing the *sst1.1* plasmid. We thank Vincent Guillemot from the ICM Biostatistics/Bioinformatics core facility for advices on statistics and the imaging facility PICPS from ICM. This work received support from the ERC starting grant

'Optoloco' #311673, the ATIP/Avenir program supported by the Fondation Bettencourt-Schueller, the Emergence program grant of the city of Paris and the HFSP research grant #RGP0063/2014. ICM facilities received support of the 'Investissements d'avenir' ANR-10-IAIHU-06.

Author Contributions

Lydia D. performed *in situ* hybridization, injected DNA constructs, performed IHCs, reconstructed cell morphology to complete the analysis of axonal projections with the help of J.G. and A.P., and the mapping of CSF-cN targets. Laura D. performed IHCs to complete the morphological analysis on CSF-cN apical extension. J.G. and J.R.S. performed the 5-HT and GABA IHC respectively. J.P.R. performed the EM analysis of CSF-cNs with the technical assistance of D.L., J.G. and Lydia D. F.B.Q. and H.M. performed additional *in situ* hybridization at later larval stages and in the adult zebrafish. Lydia D., J.G. and J.R.S. counted cells. J.R.S. performed the optogenetic stimulation of CSF-cNs and the electrophysiological recordings of CaPs. TOA generated the transgenic *icm22* line. C.W., P.L.B. and F.D.B. supervised research. Lydia D. and C.W. wrote the manuscript with feedback from all authors.

Additional Information

Supplementary information accompanies this paper at doi:10.1038/s41598-017-00350-1

Competing Interests: The authors declare that they have no competing interests.

Publisher's note: Springer Nature remains neutral with regard to jurisdictional claims in published maps and institutional affiliations.

Open Access This article is licensed under a Creative Commons Attribution 4.0 International License, which permits use, sharing, adaptation, distribution and reproduction in any medium or format, as long as you give appropriate credit to the original author(s) and the source, provide a link to the Creative Commons license, and indicate if changes were made. The images or other third party material in this article are included in the article's Creative Commons license, unless indicated otherwise in a credit line to the material. If material is not included in the article's Creative Commons license and your intended use is not permitted by statutory regulation or exceeds the permitted use, you will need to obtain permission directly from the copyright holder. To view a copy of this license, visit http://creativecommons.org/licenses/by/4.0/.

© The Author(s) 2017